

# Cryogenic Helium Adsorbed in Zeolite Rho: Inside Localization Controlled Self-Diffusion of Confined Quantum Particles

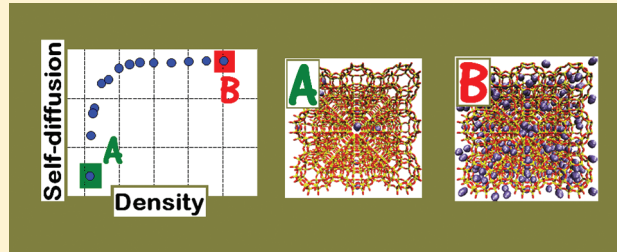
Piotr Kowalczyk,<sup>\*,†</sup> Piotr A. Gauden,<sup>‡</sup> Artur P. Terzyk,<sup>‡</sup> Sylwester Furmaniak,<sup>‡</sup> and Katsumi Kaneko<sup>§</sup>

<sup>†</sup>Nanochemistry Research Institute, Department of Chemistry, Curtin University of Technology, P.O. Box U1987, Perth, 6845 Western Australia, Australia

<sup>‡</sup>Department of Chemistry, Physicochemistry of Carbon Materials Research Group, N. Copernicus University, Gagarin St. 7, 87-100 Torun, Poland

<sup>§</sup>Research Center for Exotic Nanocarbons (JST), Shinshu University, 4-17-1 Wakasato, Nagano-city, Nagano 380-8553, Japan

**ABSTRACT:** Applying Feynman's treatment of quantum mechanics at finite temperatures via path integrals and the numerical analytic continuation method developed recently (Kowalczyk, P.; Gauden, P. A.; Terzyk, A. P.; Furmaniak, Sylwester, *J. Chem. Theory Comput.* 2009, 5, 1990–1996), we study the mobility of <sup>4</sup>He atoms adsorbed in zeolite rho at 40 K. At studied temperature, the self-diffusive motion of <sup>4</sup>He atoms in zeolite rho is strongly concentration-dependent. At low pore concentrations, <sup>4</sup>He atoms are adsorbed in high-energetic adsorption centers of the zeolite. Due to strong localization in the solid–fluid potential well, an average kinetic energy of <sup>4</sup>He atoms at infinite dilution reaches ~120 K (i.e., twice of the classical kinetic energy at 40 K,  $E_{\text{class}} = 60 \text{ K}$ ), whereas the self-diffusion constant drops up to ~0.001 Å<sup>2</sup> ps<sup>-1</sup>. Increasing pore concentration of <sup>4</sup>He leads to the rapid increase in mobility of adsorbed <sup>4</sup>He atoms. We show that ~8 mmol cm<sup>-3</sup>, self-diffusive motion of confined <sup>4</sup>He atoms increases up to ~1 Å<sup>2</sup> ps<sup>-1</sup>. Variation of the kinetic energy, potential energy, and enthalpy of <sup>4</sup>He adsorption with pore concentration indicates that high-energetic adsorption sites in studied zeolite sample are saturated at low pore densities. The remaining adsorption sites are characterized by weaker solid–fluid potential, which allows higher delocalization of adsorbed <sup>4</sup>He atoms. The reported novel phenomenon of localization controlled self-diffusion of confined <sup>4</sup>He seems to be promising for smart designing of nanoporous quantum molecular sieves and storage nanovessels. Understanding of <sup>4</sup>He cryogenic adsorption in the smallest pores enriches our knowledge that is crucial for precise analysis of ultramicropore sizes.



## 1. INTRODUCTION

Detailed understanding of mobility of sorbates in nanoporous materials is important for developing applications involving membrane and pressure swing separations.<sup>1–4</sup> While self-diffusion of classical fluids as well as their mixtures in various porous materials, including zeolites, has been studied extensively, both theoretically and experimentally,<sup>5–25</sup> there are very few studies of quantum fluid self-diffusion in nanopores at cryogenic temperatures.<sup>26–30</sup> Accurate prediction of dynamical properties of light particles adsorbed in nanopores (i.e., exposed to strong and nonuniform solid–fluid potential) at very low temperatures is a challenging problem. This is because when the de Broglie thermal wavelength is comparable to the size of the confined nanopores and to the distances between adsorbed/compressed particles, the consideration of quantum effects (i.e., zero-point energy and tunneling) in theoretical models and molecular simulations is absolutely crucial.<sup>31–40</sup>

To the best of our knowledge, only Feynman–Hibbs (FH) effective potentials have been used to study the dynamic properties of quantum fluids confined in nanopores at cryogenic temperatures.<sup>26–30</sup> These semiclassical methods are very easy to implement in conventional Newtonian molecular dynamics

codes because they use the concept of the molecular trajectory in a phase-space.<sup>41</sup> However, there are no definite positions of quantum particles according to fundamental Heisenberg's uncertainty principle.<sup>42</sup> As theoretically justified, FH effective potentials are only exact in the short-time limit, when the time of dynamics  $t \ll \omega^{-1}$ , where  $\omega$  denotes the Einstein frequency.<sup>38,42</sup> Thus we see that semiclassical FH effective potentials correctly describe the real dynamics of quantum particles only before any collisions have taken place within the system. In practical applications, we are interested in probing of quantum dynamics on the time scales that are far beyond the collision frequency. As shown by Sesé,<sup>43,44</sup> when the reduced de Broglie thermal wavelength  $\Lambda^* \equiv h/(2\pi m k_b T \omega_H^{2/3})^{1/2} \leq 0.5$ , FH effective potentials are able to reproduce static and thermodynamics properties of homogenous quantum fluids computed from exact path integral simulations. Following to results displayed in Table 1, we concluded that at 40 K the FH short-time approximation is questionable for description of thermodynamic and

**Received:** May 27, 2011

**Revised:** July 15, 2011

**Published:** August 29, 2011

**Table 1.** Temperature Variation of de Reduced Broglie Thermal Wavelength,  $\Lambda^* \equiv h/(2\pi m k_b T \sigma_{\text{eff}}^2)^{1/2}$ , for Selected Quantum Adsorbates

particle	temperature (K)			
	20	30	40	77
<sup>4</sup> He	0.76	0.62	0.54	0.39
H <sub>2</sub>	0.93	0.76	0.66	0.47
D <sub>2</sub>	0.66	0.54	0.46	0.34
Ne	0.31	0.25	0.22	0.16

static properties of homogenous <sup>4</sup>He and H<sub>2</sub> fluids. Because strong confinement shifts the phase diagram for simple quantum fluids<sup>45–49</sup> (i.e., adsorbed fluid is very dense and highly compressed in nanopores composed of attractive pore walls), we would expect that FH effective potentials are poor approximation for heavier particles, such as D<sub>2</sub> fluid adsorbed in nanopores at 40 K. Finally, we want to stress that Sesé criterion does not consider any dynamical properties of quantum fluids, such as self-diffusion coefficient. Thus, the simplified FH treatment of quantum dynamics at finite temperatures for  $\Lambda^* \leq 0.5$  seems to be ad hoc assumption.

Since its original formulation in 1948, Feynman's path integral representation of time-dependent quantum mechanics has provided a powerful tool for studying many-body problems at finite temperatures without introducing uncontrolled approximations.<sup>50–58</sup> While computing equilibrium properties at finite temperatures via path integrals has become routine, the calculation of dynamical properties from path integrals remains one of the most challenging problems in computational chemistry and physics. This is because path integral calculations in imaginary time converge on time scales similar to those of classical calculations. Unfortunately, the same is not true for the quantum propagator in real time due to the complex exponential in the action's integrand.<sup>38</sup> In 2010, Tuckerman wrote in his book:<sup>38</sup> “As of the writing of this book, no truly satisfactory solution has been achieved”.

To best of our knowledge numerical analytic continuation method (NAC),<sup>40,59,60</sup> centroid molecular dynamics (CMD),<sup>61–63</sup> ring molecular dynamics (RMD),<sup>64–66</sup> and quantum version of model-coupling theory (QMCT)<sup>52,67,68</sup> are the most promising methods used for the computation of self-diffusive coefficients for quantum fluids in the Boltzmann region. NAC is, in principle, an exact method that has been successfully used to study various homogeneous and inhomogeneous quantum fluids at finite temperatures.<sup>30,59,60</sup> Recent study of Rabani and co-workers<sup>40</sup> showed that all aforementioned methods yielded similar self-diffusion constants (i.e., zero time value of the velocity autocorrelation) for normal liquid <sup>4</sup>He at 4 K. Thus, in the current work we used original implementation of NAC approach developed recently<sup>60</sup> to answer the following questions: How do quantum effects modify the self-diffusive motion of <sup>4</sup>He at low temperatures?, How does zeolite energetic heterogeneity impact the localization and self-diffusive motion of adsorbed <sup>4</sup>He atoms? In Section 2, we present all computational details including: molecular models, simulation procedures, and definition of thermodynamic and dynamic quantities used in the current work. Next, we present discussion of simulation results. We concentrate our discussion on the variation of the <sup>4</sup>He self-diffusion coefficient with the pore concentration.

## 2. SIMULATION DETAILS

**2.1. Path Integral Action.** According to Feynman's path integral formalism we mapped each <sup>4</sup>He atom onto an equivalent polymer chain or ‘necklace’ of  $P$  classical ‘beads’  $\mathbf{r}_i^{(1)}, \mathbf{r}_i^{(2)}, \dots, \mathbf{r}_i^{(P)}$ .<sup>41</sup> The vector  $\mathbf{r}$  denotes the position of a bead belonging to the  $i$ -th molecule. In our simulations of <sup>4</sup>He in zeolite rho, we have used the primitive action, given by the following:<sup>31,32</sup>

$$W = \frac{mP}{2\beta^2 \hbar^2} \sum_{i=1}^N \sum_{\alpha=1}^P (\mathbf{r}_i^{(\alpha)} - \mathbf{r}_i^{(\alpha+1)})^2 + \frac{1}{P} \sum_{i < j} \sum_{\alpha=1}^P V_{ff}(\mathbf{r}_{ij}^{(\alpha)}) + \frac{1}{P} \sum_{i=1}^N \sum_{\alpha=1}^P V_{sf}(\mathbf{r}_i^{(\alpha)}) \quad (1)$$

where  $N$  is the number of <sup>4</sup>He atoms,  $\beta = (k_B T)^{-1}$  is the inverse of the temperature,  $m$  denotes mass of <sup>4</sup>He, and  $\hbar$  is Planck's constant divided by  $2\pi$ . Owing to the cyclic condition of the polymer chains, if  $\alpha = P$ , then  $\alpha + 1 = 1$ . The interaction potential between <sup>4</sup>He atoms,  $V_{ff}(r)$ , is taken from Aziz et al.<sup>69</sup> As previously,<sup>60</sup> in all performed path integral Monte Carlo simulations we quantized <sup>4</sup>He by 128 beads. The (12,6) Lennard-Jones potential was used to calculate the interactions between <sup>4</sup>He and the zeolite framework atoms. For oxygen we used  $\sigma_{\text{O-O}} = 3.3 \text{ \AA}$  and  $\varepsilon_{\text{O-O}}/k_b T = 82.98 \text{ K}$ , whereas for silicon we adopted  $\sigma_{\text{Si-Si}} = 4.2 \text{ \AA}$  and  $\varepsilon_{\text{Si-Si}}/k_b T = 23.61 \text{ K}$ .<sup>70</sup> As previously,<sup>55</sup> for <sup>4</sup>He we used  $\sigma_{\text{He-He}} = 2.556 \text{ \AA}$  and  $\varepsilon_{\text{He-He}}/k_b T = 10.22 \text{ K}$ . The cross terms for the Lennard-Jones parameters were determined using Lorentz-Berthelot mixing rules.<sup>71,72</sup>

**2.2. Grand Canonical Path Integral Monte Carlo Method.** We used grand canonical path integral Monte Carlo simulation technique (PIGCMC)<sup>73,74</sup> to generate initial configurations of <sup>4</sup>He atoms adsorbed in zeolite rho at 40 K. The chemical potential computed from Widom's particle insertion method<sup>75,76</sup> in canonical ensemble was an input in the PIGCMC simulations. The zeolite rho framework topology used in this investigation was taken from Accelrys' Materials Studio crystal structure database. The zeolite rho structure (centrosymmetric space group  $Im\bar{3}m$ ) was assumed to be rigid during the sorption process. We used a large simulation box with the cubic unit cell dimension of 4.35 nm, and periodic boundary conditions, applied in three-dimensions in order to simulate an infinite system. As in our previous studies, fluid-fluid interactions between the adsorbed molecules were cut off at  $r_{\text{cut}} = 5\sigma_{\text{He}}$  ( $\sigma_{\text{He}} = 2.556 \text{ \AA}$ ).<sup>60</sup> Thermalization of the adsorbed <sup>4</sup>He is performed by path-displacement trials (i.e., centroid displacement and bisection) whereas chemical equilibration between adsorbed <sup>4</sup>He and the reservoir is realized by the patch-exchange trials.<sup>73,74</sup> The acceptance probabilities are given by the Metropolis algorithm.<sup>73,74</sup> In all PIGCMC simulations,  $10^8$  configurations were used, of which we discarded the first  $6 \times 10^7$  to guarantee equilibration. The stability of the simulation results was confirmed by additional longer runs of  $5 \times 10^8$  configurations. The equilibrium configurations of <sup>4</sup>He classical counterpart were obtained from PIGCMC simulation in the classical limit (i.e., for the number of beads  $P = 1$  in eq 1).<sup>73,74</sup> Absolute value and enthalpy of <sup>4</sup>He adsorption was computed using energy/particle fluctuations in grand canonical ensemble.<sup>73,74</sup>

**2.3. Canonical Path Integral Monte Carlo Method.** In order to obtain imaginary-time correlation functions, we have performed a series of path integral simulations in NVT ensemble.<sup>71,72</sup>

In our simulations, we used at least 80 adsorbed  $^4\text{He}$  atoms interacting via spherically symmetric potential due to Aziz et al.<sup>69</sup> All initial  $^4\text{He}$  configurations were taken from PIGCMC simulations. For each studied system we performed  $2 \times 10^6$  Monte Carlo steps using the staging algorithm.<sup>31,32</sup> The kinetic and potential energy was computed from thermodynamics estimator.<sup>59,60</sup>

**2.4. Frequency-Dependent Diffusion Constant.** As previously,<sup>60</sup> we determined the frequency-dependent diffusion constant,  $D(\omega)$ , from the following integral equation,

$$G_v(\tau) = \frac{1}{2\pi} \int_0^\infty [e^{-\omega\tau} + e^{-(\tau-\beta)\omega}] D(\omega) d\omega \quad (2)$$

where  $G_v(\tau)$  denotes the imaginary-time correlation function,  $\beta = (k_B T)^{-1}$  is the inverse temperature,  $0 < \tau < \beta$  is the imaginary time.

We computed imaginary-time correlation function from PIMC simulations in the canonical ensemble,<sup>59,60</sup>

$$G_v(\tau_j) = \delta_{j1} \frac{1}{3m\varepsilon} - \frac{1}{N\varepsilon^2} \sum_{\alpha=1}^N \int d\mathbf{r}_1 \cdots d\mathbf{r}_P P(\mathbf{r}_1, \dots, \mathbf{r}_P) \times (\mathbf{r}_\alpha^j - \mathbf{r}_\alpha^{j-1}) \cdot (\mathbf{r}_\alpha^2 - \mathbf{r}_\alpha^1) \quad (3)$$

where  $\delta$  is the Kronecker delta function,  $\varepsilon = \beta/P$ ,  $N$  is the total number of particles,  $P$  denotes the number of beads,  $\mathbf{r}_j$  is a shorthand notation for the position vectors of all particles assisted with bead  $j$ ,  $\mathbf{r}_\alpha^j$  is the position vector of liquid particle  $\alpha$  of bead  $j$  and  $P(\mathbf{r}_1, \dots, \mathbf{r}_P)$  is the regular sampling function used in standard cyclic PIMC method (with  $\mathbf{r}_0 = \mathbf{r}_P$ ).<sup>59,60</sup> In our PIMC, imaginary-time correlation function was collected every 10 configurations. According to our previous works,<sup>30,60</sup> we inverted ill-posed integral equation given by eq 2 by using first-order Tikhonov's regularizing functional.

### 3. RESULTS AND DISCUSSION

Of all quantum liquids,  $^4\text{He}$  is the most common and characteristic one. It is, therefore, an ideal system for investigating the microscopic origin of quantum effects and for doing comparisons between experiments and theory.<sup>31,32,55</sup> Figure 1 depicts adsorption isotherm and enthalpy of  $^4\text{He}$  adsorption in zeolite rho at 40 K. For comparison, we computed these fundamental adsorption characteristics for  $^4\text{He}$  classical counterpart. Regardless of the pore density, we found that classical treatment of  $^4\text{He}$  atoms results in higher adsorbed amount and enthalpy of  $^4\text{He}$  adsorption at 40 K. As would be expected,<sup>46,47</sup> quantum fluctuations destabilize high density phases in nanopores that reduce the packing of  $^4\text{He}$  atoms in zeolite rho. As compared to classical simulations, we notice that the excess of the kinetic energy of adsorbed  $^4\text{He}$  atoms is responsible for the reduction of the enthalpy of  $^4\text{He}$  adsorption at cryogenic temperatures. Interestingly, we found that both variation of adsorbed amount and enthalpy of  $^4\text{He}$  adsorption in zeolite rho are regularly shifted to lower values by quantum fluctuations. This indicates that whatever the  $^4\text{He}$  atoms are treated classically or quantum-mechanically the adsorption mechanism is very similar for studied operating conditions. Thus, both  $^4\text{He}$  atoms and their classical counterparts are initially adsorbing in high-energetic adsorption centers of zeolite rho (see Figures 1-2). With the adsorption process progressing, the enthalpy of  $^4\text{He}$  adsorption is monotonically decreasing because adsorbed  $^4\text{He}$

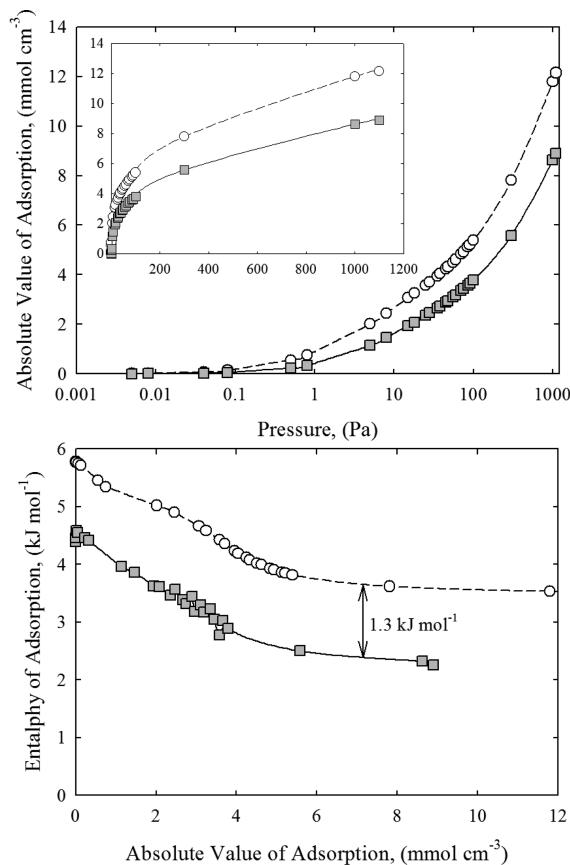


**Figure 1.** Upper panel: pressure variation of the absolute value of  $^4\text{He}$  adsorption in zeolite rho at 40 K computed from path integral GCMC (closed squares) and classical GCMC (open spheres) simulations. Lower panel: Decreasing of the enthalpy of  $^4\text{He}$  adsorption in zeolite rho at 40 K with pore loading computed from path integral GCMC (closed squares) and classical GCMC (open spheres) simulations.

atoms as well as their classical counterparts experience the weaker solid–fluid potential.

From thermodynamic properties of adsorbed  $^4\text{He}$  fluid, we expected a decreasing of  $^4\text{He}$  localization with pore loading at studied operating conditions. Indeed, frequency-dependent power spectra presented in Figure 3 confirm our expectations. For low  $^4\text{He}$  pore concentrations, we notice a significant blueshift in the position of the maximum of  $D(\omega)$ , an increase in the phonon density of states at intermediate and high frequencies, and a decrease in the phonon density of states at low frequencies. A drop in the self-diffusion constant (i.e., the drop in zero frequency absorption) is matched by the appearance of a peak at finite frequencies, and the position of this peak increases as the self-diffusion constant decreases. Why self-diffusive motion of  $^4\text{He}$  in zeolite rho at 40 K increases with pore loading? One should rather expect that crowding of adsorbed/compressed atoms (i.e., stronger localization in position space due to fluid–fluid interactions) slows down their self-diffusion.<sup>30</sup> This is not the case because we study the low-temperature adsorption processes in energetically heterogeneous zeolite crystal. At very low temperatures and pore concentrations, the solid–fluid potential seems to be the most important factor that affects the mobility of adsorbed quantum particles.

In order to explain an increasing of  $^4\text{He}$  self-diffusivity with pore loading, we carefully analyzed the variation of the potential

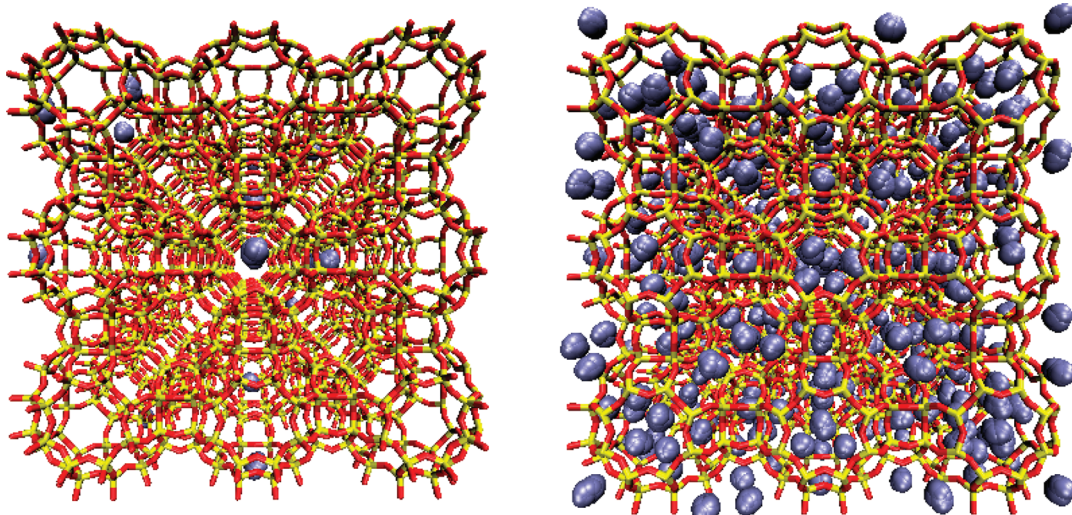


**Figure 2.** Snapshots of  $^4\text{He}$  adsorbed in zeolite rho at 40 K. Left panel corresponds to external pressure of 1 Pa, whereas right panel to 1000 Pa. Note that each delocalized  $^4\text{He}$  atom is quantized by 128 beads.

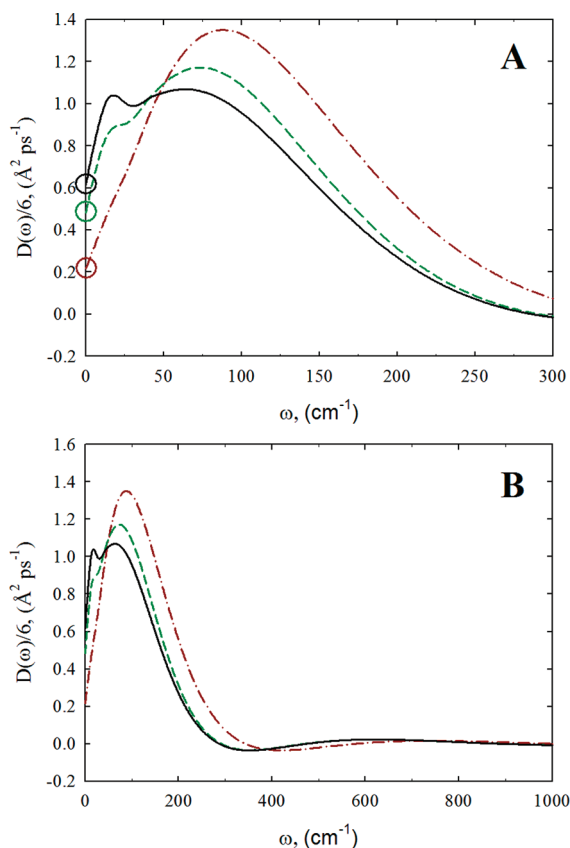


**Figure 3.** Plots of frequency-dependent diffusion constant for  $^4\text{He}$  adsorbed in zeolite rho at 40 K. Studied pore densities are as follows: 1.4 (dotted-dashed red line), 2.6 (dashed green line), and 8.1 (solid black line)  $\text{mmol cm}^{-3}$ . Panel A corresponds to the region of low frequencies, with self-diffusion constants marked by open spheres.

and kinetic energy of  $^4\text{He}$  atoms adsorbed in zeolite rho with pore loading at 40 K, as is shown in Figure 4. First, we notice that variation of self-diffusion constant with  $^4\text{He}$  pore density follows Type III self-diffusion processes according to Kärger–Pfeifer

classification.<sup>13</sup> Second, we observe a concentration-dependent decrease and increase in kinetic and potential energy, respectively. Since  $^4\text{He}$  atoms are preferentially adsorbed at the strongest adsorption sites (see top panel in Figure 4) at low pore concentrations, with increase in pore loading the relative number of strong adsorption binding sites will decrease, as a result, the overall self-diffusivity of adsorbed  $^4\text{He}$  atoms will increase. The very high kinetic energy of  $^4\text{He}$  atoms at low pore densities indicates a strong localization of quantum particles by the high-energetic adsorption sites (see left panel in Figure 2). It is worth to underline that strong enhancement of kinetic energy of  $^4\text{He}$  as well as Ne atoms adsorbed in nanoporous materials was directly measured from the neutron Compton scattering technique. Nemirovsky et al.<sup>77,78</sup> found that the average kinetic energy of  $^4\text{He}$  atoms confined in nanoporous activated carbon fibers reached 53 at 10.2 K. For the same operating temperature, the classical kinetic energy is only 15.3 K. The high excess of kinetic energy results from strong localization of  $^4\text{He}$  atoms inside slit-shaped graphitic nanopores. Interestingly, we found that above  $\sim 3 \text{ mmol cm}^{-3}$ , both kinetic energy and self-diffusion constant of confined  $^4\text{He}$  atoms at 40 K is stabilized. This simply indicates that strong adsorption binding sites in zeolite rho is saturated by  $^4\text{He}$  atoms at low pore densities, whereas the remaining adsorption sites are characterized by similar adsorption affinity. The fact that the self-diffusive motion of  $^4\text{He}$  atoms strongly depends on their localization is not only interesting theoretical result, but also seems to be very promising for smart designing of nanoporous quantum molecular sieves as well as for ultramicropore size analysis. With sufficiently developed atomistic level theory and precise experiment, one can optimize the separation of quantum particles from their mixtures by selective permeation through nanoporous materials (known as nanoporous quantum filters). Moreover as suggested by Nemirovsky et al.,<sup>77,78</sup> an average kinetic energy of adsorbed  $^4\text{He}$  atoms can be correlated with the size of ultramicropore. This is because a strong nanoconfinement strongly impact on the localization of quantum particle, as is shown in Figure 4. Prediction of kinetic molecular sieving of model quantum mixtures will be subject of our future studies.

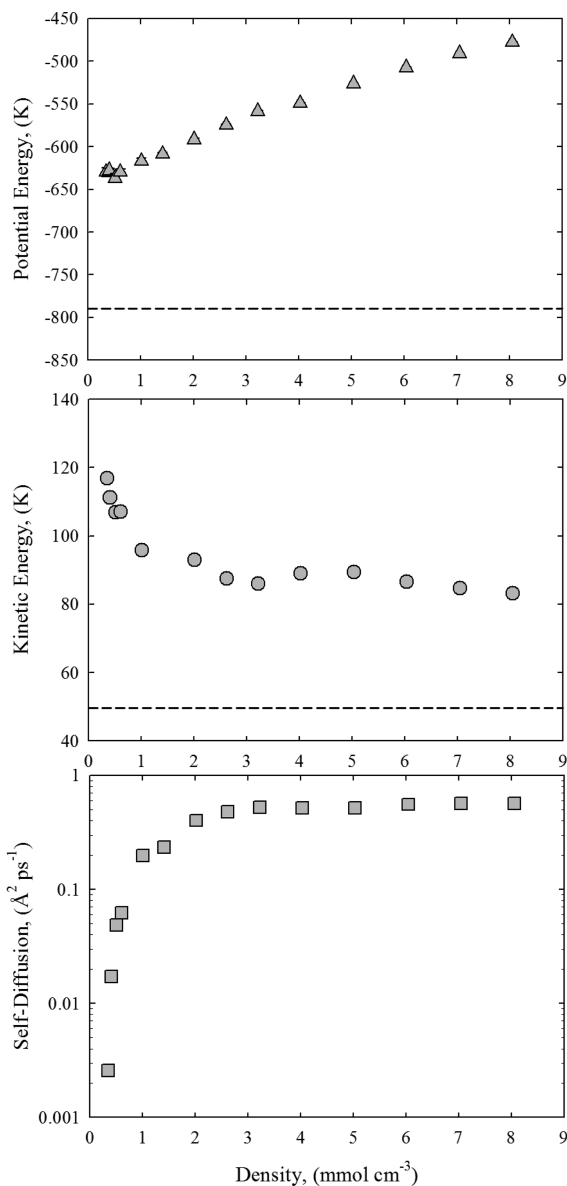


**Figure 4.** Pore density variation of potential energy (upper panel), kinetic energy (middle panel), and self-diffusion constant (bottom panel) for  ${}^4\text{He}$  adsorbed in zeolite rho at 40 K. Dashed lines correspond to classical kinetic and potential energy.

## 4. CONCLUSIONS

We study the mobility of  ${}^4\text{He}$  atoms adsorbed in zeolite rho up to  $\sim 8 \text{ mmol cm}^{-3}$  at 40 K. Path integral calculations showed that self-diffusive motion of  ${}^4\text{He}$  atoms adsorbed in zeolite rho at studied cryogenic temperature is strongly concentration-dependent. At low pore densities,  ${}^4\text{He}$  atoms are localized in high-energetic centers of host material that is confirmed by their high average value of kinetic energy ( $\sim 120 \text{ K}$ ). At infinite dilution, the mobility of adsorbed  ${}^4\text{He}$  atoms are very small (i.e., their self-diffusion coefficient drops up to  $\sim 0.001 \text{ \AA}^2 \text{ ps}^{-1}$ ). Increasing in  ${}^4\text{He}$  pore loading is accompanied by rapid increasing in mobility of adsorbed  ${}^4\text{He}$  atoms. At  $\sim 8 \text{ mmol cm}^{-3}$ , self-diffusive motion of confined  ${}^4\text{He}$  atoms is increased up to  $\sim 1 \text{ \AA}^2 \text{ ps}^{-1}$ . Variation of kinetic energy, enthalpy of  ${}^4\text{He}$  adsorption, and self-diffusion constant with pore concentration indicate that high-energetic

adsorption sites are saturated around  $\sim 3 \text{ mmol cm}^{-3}$ . The remaining adsorption sites are characterized by weaker solid–fluid potential, which allows higher delocalization of adsorbed  ${}^4\text{He}$  atoms. Localization controlled self-diffusion of confined  ${}^4\text{He}$  seems to be a promising phenomenon used for smart designing of nanoporous quantum molecular sieves and storage nanovessels. It can also be used for determination of ultramicropore sizes from low temperature  ${}^4\text{He}$  adsorption measurements.

## ■ AUTHOR INFORMATION

### Corresponding Author

\*Tel: +61 8 9266 7800; E-mail: Piotr.Kowalczyk@curtin.edu.au.

## ■ ACKNOWLEDGMENT

P.K. acknowledges partial support by the Office of Research & Development, Curtin University of Technology, Grant CRF10084. P.K. acknowledges partial support by the Australian Academy of Science, Scientific Visits to Japan 2011-12 Grant. P.A.G. acknowledges the use of the computer cluster at Poznan Supercomputing and Networking Centre as well as the Information and Communication Technology Centre of the Nicolaus Copernicus University (Torun, Poland). K.K. was supported by Exotic Nanocarbons, Japan Regional Innovation Strategy Program by the Excellence, JST.

## ■ REFERENCES

- (1) Auerbach, S. M.; Carrado, K. A.; Dutta, P. K. *Handbook of Zeolite Science and Technology*; Marcel Dekker, Inc.: New York, 2003.
- (2) Yang, R. T. *Gas Separation by Adsorption Processes*; Imperial College Press: London, 1997.
- (3) Do, D. D. *Adsorption Analysis: Equilibria and Kinetics*; ICP: London, 1998.
- (4) Marsh, H.; Rodriguez-Reinoso, F. *Activated Carbon*; Elsevier Ltd.: Oxford, 2006.
- (5) Käger, J.; Ruthven, D. M. *Diffusion in Zeolites and Other Microporous Solids*; John Wiley & Sons: New York, 1992.
- (6) Jobic, H.; Käger, J.; Bée, M. *Phys. Rev. Lett.* **1999**, *82*, 4260–4263.
- (7) Sant, N.; Leyssale, J.-M.; Papadopoulos, G. K.; Theodorou, D. N. *J. Phys. Chem. B* **2009**, *113*, 13761–13767.
- (8) Jobic, H.; Theodorou, D. N. *J. Phys. Chem. B* **2006**, *110*, 1964–1967.
- (9) Jobic, H.; Theodorou, D. N. *Microporous Mesoporous Mater.* **2007**, *102*, 21–50.
- (10) Käger, J. *Adsorption* **2003**, *9*, 29–35.
- (11) Brandani, S.; Ruthven, D. M.; Käger, J. *Zeolites* **1995**, *15*, 494–496.
- (12) Nelson, P. H.; Auerbach, S. M. *J. Chem. Phys.* **1999**, *110*, 9235–9243.
- (13) Käger, J.; Pfeifer, H. *Zeolites* **1987**, *7*, 90–107.
- (14) Krishna, R.; van Baten, J. M. *Langmuir* **2010**, *26*, 2975–2978.
- (15) Krishna, R.; van Baten, J. M. *Langmuir* **2010**, *26*, 3981–3992.
- (16) Krishna, R.; van Baten, J. M. *J. Phys. Chem. C* **2010**, *114*, 18017–18021.
- (17) Krishna, R.; van Baten, J. M. *Microporous Mesoporous Mater.* **2008**, *107*, 296–298.
- (18) Dubbeldam, D.; Beerdsen, E.; Calero, S.; Smit, B. *Proc. Natl. Acad. Sci. U.S.A.* **2005**, *102*, 12317–12320.
- (19) Beerdsen, E.; Dubbeldam, D.; Smit, B. *Phys. Rev. Lett.* **2006**, *96*, 044501.
- (20) Kowalczyk, P.; Gauden, P. A.; Terzyk, A. P.; Furmaniak, S. *Phys. Chem. Chem. Phys.* **2010**, *12*, 11351–11361.

- (21) Jakobtorweihen, S.; Verbeek, M. G.; Lowe, C. P.; Keil, F. J.; Smit, B. *Phys. Rev. Lett.* **2005**, *95*, 044501.
- (22) Snurr, R. Q.; Kärger, J. *J. Phys. Chem. B* **1997**, *101*, 6469–6473.
- (23) Heuchel, M.; Snurr, R. Q.; Buss, E. *Langmuir* **1997**, *13*, 6795–6804.
- (24) Ruthven, D. M. *Principles of Adsorption and Adsorption Processes*; John Wiley & Sons: New York, 1984.
- (25) Theodorou, D. M. *Ind. Eng. Chem. Res.* **2010**, *49*, 3047–3058.
- (26) Pantatosaki, E.; Papadopoulos, G. K. *J. Chem. Phys.* **2007**, *127*, 164723.
- (27) Nguyen, T. X.; Jobic, H.; Bhatia, S. K. *Phys. Rev. Lett.* **2010**, *105*, 085901.
- (28) Pantatosaki, E.; Papadopoulos, G. K.; Jobic, H.; Theodorou, D. N. *J. Phys. Chem. B* **2008**, *112*, 11708–11715.
- (29) Pantatosaki, E.; Pazzona, F. G.; Megariotis, G.; Papadopoulos, G. K. *J. Phys. Chem. B* **2010**, *114*, 2493–2503.
- (30) Kowalczyk, P.; Gauden, P. A.; Terzyk, A. P.; Furmaniak, S. *Phys. Chem. Chem. Phys.* **2011**, *13*, 9824–9830.
- (31) Ceperley, D. M. *Rev. Mod. Phys.* **1995**, *67*, 279–356.
- (32) Ceperley, D. M. *Rev. Mod. Phys.* **1999**, *71*, S438–S443.
- (33) Hone, T. D.; Poulsen, J. A.; Rossky, P. J.; Manolopoulos, D. E. *J. Phys. Chem. B* **2008**, *112*, 294–300.
- (34) Habershon, S.; Braams, B. J.; Manolopoulos, D. E. *J. Chem. Phys.* **2007**, *127*, 174108.
- (35) Hone, T. D.; Rossky, P. J.; Voth, G. A. *J. Chem. Phys.* **2006**, *124*, 154103.
- (36) Tuckerman, M. E.; Martyna, G. J.; Klein, M. L.; Berne, B. J. *J. Chem. Phys.* **1993**, *99*, 2796–2808.
- (37) Berne, B. J. *J. Stat. Phys.* **1986**, *43*, 911–929.
- (38) Tuckerman, M. E. *Statistical Mechanics: Theory and Molecular Simulation*; Oxford University Press: Oxford, 2010.
- (39) Kowalczyk, P.; Holyst, R.; Terrones, M.; Terrones, H. *Phys. Chem. Chem. Phys.* **2007**, *9*, 1786–1792.
- (40) Rabani, E.; Krilov, G.; Reichman, D. R.; Berne, B. J. *J. Chem. Phys.* **2005**, *123*, 184506.
- (41) Feynman, R. P.; Hibbs, A. *Quantum Mechanics and Path Integrals*; McGraw-Hill: New York, 1965.
- (42) Dirac, P. *The Principles of Quantum Mechanic*; Oxford University Press: New York, 1982.
- (43) Sesé, L. M. *Mol. Phys.* **1994**, *81*, 1297–1312.
- (44) Sesé, L. M. *Mol. Phys.* **1995**, *85*, 931–947.
- (45) Kowalczyk, P.; Tanaka, H.; Holyst, R.; Kaneko, K.; Ohmori, T.; Miyamoto, J. *J. Phys. Chem. B* **2005**, *109*, 17174–17183.
- (46) Hoffmann, J.; Nielaba, P. *Phys. Rev. E* **2003**, *67*, 036115.
- (47) Kowalczyk, P.; Gauden, P. A.; Terzyk, A. P. *J. Phys. Chem. B* **2010**, *114*, 5047–5052.
- (48) Gelb, L. D.; Gubbins, K. E.; Radhakrishnan, R.; Sliwinska-Bartkowiak, M. *Rep. Prog. Phys.* **1999**, *62*, 1573–1659.
- (49) Kowalczyk, P.; Solarz, L.; Do, D. D.; Samborski, A.; MacElroy, J. M. *Langmuir* **2006**, *22*, 9035–9040.
- (50) Feynman, R. P. *Feynman's Thesis—A New Approach to Quantum Theory*; edited by Brown, L. M.; World Scientific Publishing Company: Singapore, 2005.
- (51) Berne, B. J.; Thirumalai, D. *Annu. Rev. Phys. Chem.* **1986**, *37*, 401–424.
- (52) Rabani, E.; Reichman, D. R. *Annu. Rev. Phys. Chem.* **2005**, *56*, 157–185.
- (53) Kinugawa, K.; Moore, P. B.; Klein, M. L. *J. Chem. Phys.* **1998**, *109*, 610–617.
- (54) Tuckerman, M. E.; Marx, D.; Klein, M. L.; Parrinello, M. *Science* **1997**, *275*, 817–820.
- (55) Kowalczyk, P.; Brualla, L.; Gauden, P. A.; Terzyk, A. P. *Phys. Chem. Chem. Phys.* **2009**, *11*, 9182–9187.
- (56) Kletenik-Edelman, O.; Rabani, E.; Reichman, D. R. *Chem. Phys.* **2010**, *370*, 132–136.
- (57) Kletenik-Edelman, O.; Reichman, D. R.; Rabani, E. *J. Chem. Phys.* **2011**, *134*, 044528.
- (58) Nakayama, A.; Makri, N. *Proc. Natl. Acad. Sci. U.S.A.* **2005**, *102*, 4230–4234.
- (59) Rabani, E.; Reichman, D. R.; Krilov, G.; Berne, B. J. *Proc. Natl. Acad. Sci. U.S.A.* **2002**, *99*, 1129–1133.
- (60) Kowalczyk, P.; Gauden, P. A.; Terzyk, A. P.; Furmaniak, S. *J. Chem. Theory Comput.* **2009**, *5*, 1990–1996.
- (61) Cao, J.; Voth, G. A. *J. Chem. Phys.* **1993**, *99*, 10070–10073.
- (62) Cao, J.; Voth, G. A. *J. Chem. Phys.* **1994**, *100*, 5106–5117.
- (63) Cao, J.; Voth, G. A. *J. Chem. Phys.* **1994**, *101*, 6168–6183.
- (64) Craig, I. R.; Manolopoulos, D. E. *J. Chem. Phys.* **2004**, *121*, 3368–3373.
- (65) Miller, T. F.; Manolopoulos, D. E. *J. Chem. Phys.* **2005**, *123*, 154504–154504.
- (66) Habershon, S.; Markland, T. E.; Manolopoulos, D. E. *J. Chem. Phys.* **2009**, *131*, 024501.
- (67) Rabani, E.; Reichman, D. R. *J. Chem. Phys.* **2002**, *116*, 6271–6278.
- (68) Markland, T. E.; Morrone, J. A.; Berne, J. B.; Miyazaki, K.; Rabani, E.; Reichman, D. R. *Nature Physics* **2011**, *7*, 134–137.
- (69) Aziz, R. A.; Slaman, M. J.; Koide, A.; Allnatt, A. R.; Meath, W. J. *Mol. Phys.* **1992**, *77*, 321–337.
- (70) Rahmati, M.; Modarress, H. *App. Surf. Sci.* **2009**, *255*, 4773–4778.
- (71) Allen, M. P.; Tildesley, D. J. *Computer Simulation of Liquids*; Clarendon: Oxford, 1987.
- (72) Frenkel, D.; Smit, B. *Understanding Molecular Simulation From Algorithms To Applications*; Academic Press: London, 1996.
- (73) Wang, Q.; Johnson, J. K.; Broughton, J. Q. *J. Chem. Phys.* **1997**, *107*, 5108–5117.
- (74) Kowalczyk, P.; Gauden, P. A.; Terzyk, A. P.; Bhatia, S. *Langmuir* **2007**, *23*, 3666–3672.
- (75) Widom, B. *J. Chem. Phys.* **1963**, *39*, 2808–2812.
- (76) Wang, Q.; Johnson, J. K. *Fluid Phase Equilib.* **1997**, *132*, 93–116.
- (77) Nemirovsky, D.; Moreh, R.; Andersen, K. H.; Mayers, J. *J. Phys.: Condens. Matter* **1999**, *11*, 6653–6660.
- (78) Nemirovsky, D.; Moreh, R.; Kaneko, K.; Ohba, T.; Mayers, J. *Surf. Sci.* **2003**, *526*, 282–290.